Self-avoiding random surfaces: Monte Carlo study using oct-tree data-structure

1991 J. Phys. A: Math. Gen. 24 4619

(http://iopscience.iop.org/0305-4470/24/19/024)

J. Phys. A: Math. Gen. 24 (1991) 4619-4635. Printed in the UK

Self-avoiding random surfaces: Monte Carlo study using oct-tree data-structure

Julie O'Connell†, Francis Sullivan†‖, Don Libes†, E Orlandini‡, M C Tesi‡, A L Stella§‖¶ and T L Einstein§‖

† Center for Computing and Applied Mathematics, National Institute of Standards and Technology, Gaithersburg, MD 20899, USA
‡ Dipartimento di Fisica dell'Università and Sezione INFN, I-40126 Bologna, Italy
§ Department of Physics, University of Maryland, College Park, MD 20742-4111, USA

Received 26 April 1991

Abstract. Self-avoiding random surfaces on a cubic lattice are studied by extensive Monte Carlo sampling. The surfaces have empty boundary and the topology of a 2-sphere. An oct-tree data-structure allows good statistics to be obtained for surfaces whose plaquette number is up to an order of magnitude greater than in previous investigations. The new simulation strategy is explained in detail and compared with previous ones. The critical plaquette fugacity, μ^{-1}, and the entropic exponent, θ, are determined by maximum likelihood methods and by logarithmic plots of the average surface area versus fugacity. The latter approach, which produces results having much better convergence by taking advantage of the scaling properties of several runs at various fugacities, leads to the estimates $\mu = 1.729 \pm 0.036$ and $\theta = 1.500 \pm 0.026$. Linear regression estimates for the radius of gyration exponent give $\nu = 0.509 \pm 0.004$, while the asymptotic ratio of surface area over average volume enclosed approaches a finite value 3.18 ± 0.03. Our results give strong corroborating evidence that this long-controversial problem belongs to the universality class of branched polymers.

1. Introduction

Both lattice and continuum models of random surfaces (RS) have attracted much attention in the recent literature. Among the many motivations for this interest are connections with lattice gauge theories [1-3] and possible applications to problems in condensed matter physics. RS are geometrical generalizations of random walks, which play a very fundamental role in fields such as polymer physics. Indeed, from the earliest studies of RS, there has been a natural tendency to treat their statistics within the framework of schemes directly inspired by those used in polymer physics [4-7]. On the other hand, being characterized by new properties, like intrinsic curvature, genus and orientability, RS models are expected to display a much richer variety of universality classes than their random walk counterparts, so that caution must be exercised in applying schemes used for random walks.

At present, our understanding of RS models in finite dimensions relies on numerical investigations, mostly using Monte Carlo methods. As we have already mentioned,

‖ Authors to whom correspondence should be addressed.
¶ Permanent address: Dipartimento di Fisica dell'Università and Sezione INFN, I-40126 Bologna and CISM, I-35131 Padova, Italy.

0305-4470/91/194619+17$03.50

analysis of results is more delicate than for random walks. Another barrier to carrying out such investigations is the need to store a very large amount of information in order to describe the configuration of RS. This information is much greater than that normally needed in walk problems of comparable size. Thus, RS simulation is another field in which substantial progress can be made only if efficient data-structures and robust numerical methods are introduced in such a way as to allow sufficiently fast and accurate computations.

In this study we consider a model of RS on a 3D cubic lattice, i.e. the RS are constructed by gluing together elementary square plaquettes of the lattice according to the following prescription. A surface S is given by a set of $|S|$ distinct plaquettes. Each plaquette is used only once to build S, and at each of its four edges, it is connected to one and only one other plaquette. A self-avoidance constraint is imposed in the sense that not only plaquettes but also their edges (which coincide with the bonds of the 3D lattice) enter at most once in S. Corner overlaps are still allowed. We must also specify the boundary conditions and the topology. Our surfaces are closed, so that the boundary is fixed but null. It is known [8] that convergence with fixed boundary conditions is much lower than with free boundaries. We assume the topology to be that of a 2-sphere (i.e. genus 0), thereby excluding handles. An excellent review of this problem is given in [9].

There are two quantities of primary interest to us: $N(n)$, the number of possible surface configurations with $|S| = n$, and $R(n)$, the radius of gyration with respect to the centroid of each configuration, averaged over all $N(n)$ configurations with $|S| = n$. In counting, we assume that each configuration is equivalent to all others obtained by lattice translations. Thus, by surface configuration we actually imply an equivalence class of configurations which coincide under such translations. On the basis of heuristic arguments, the following asymptotic behaviours are expected at large n:

$$N(n) \sim n^{-\theta}\mu^n \tag{1}$$

and

$$R(n) \sim n^{\nu}. \tag{2}$$

The existence of the large-n limit of $n^{-1} \ln N$ can be established by generalizing a theorem of Hammersley [10] on self-avoiding walks to self-avoiding surfaces [5]. The exponent θ relates to entropic aspects, while ν can be naturally interpreted as the reciprocal of the fractal, or capacity, dimension of surfaces.

Very little exact information is available about self-avoiding RS (SARS) models such as that described above. In particular, the determination of θ, μ and ν is essentially an open question [11, 12]. A property of self-avoiding surfaces models is that they most probably collapse into non-interacting branched polymers in the limit of high dimensionality, implying $\nu = \frac{1}{4}$ and $\theta = \frac{5}{2}$ [6, 13]. Early real-space renormalization-group calculations and Flory arguments, in the style of polymer statistics, suggested that the exponent ν of SARS at low dimensionality could be distinct from that of self-avoiding branched polymers, although the two problems would share the same upper critical dimension [4].

Sterling and Greensite [14] performed the first Monte Carlo calculation in 3D for a SARS. Considering the same model described here, in a grand canonical ensemble, they estimated $\theta = 0.5 \pm 0.05$, which would seem to exclude, at least for θ, the possibility of $\theta = \frac{3}{2}$ and $\nu = \frac{1}{2}$, the values expected for branched polymers in 3D [15]. On the other

hand, in an exact enumeration up to 10 plaquettes, Redner [16] found values of θ and ν which seemed compatible with those of branched polymers. However, he did not restrict the type of boundaries nor the topology. Thus, the identification with branched polymer behaviour seems less surprising; it is reminiscent of another plaquette model discussed, e.g. in [9, 17, 18]. Further evidence for $\theta = \frac{3}{2}$ and $\nu = \frac{1}{2}$ was obtained by Glaus and Einstein [9, 19] with Monte Carlo simulations, which improved on the work of [14]. Concurrently, Karowski [20] presented Monte Carlo results for our model suggesting that the exponent ν could indeed be distinct from $\frac{1}{2}$ and instead have a value of the type first suggested by Maritan and Stella [4]. Although Karowski's approach seems less systematic than Glaus's, he did test a domain of larger n, closer to the asymptotic limit. His results thus cast doubts on the identification of the model with branched polymers.

Further stimulation to reconsider carefully this sort of problem came from the very recent prediction that closed SARS with unrestricted number of handles should enclose an average volume growing like R^3 [21]. Monte Carlo estimates reported so far of the ratio between average enclosed volume and surface area rather indicated a volume growing with a power of R close to 2 in the case of spherical topology [9, 19], as a consequence of the fact that the ratio seemed to remain finite for $n \to \infty$, and $\nu \simeq \frac{1}{2}$. It is now of particular importance to test the situation more carefully, because, if the contention of [9] and [19] is confirmed, this, in the light of what was found by Banavar *et al* [21], would reveal a very non-trivial role played by topology in determining different universality classes for SARS problems.

Because of the above somewhat unsettled situation and challenges, we decided to undertake a new Monte Carlo investigation of the model of SARS with spherical topology, based on a more efficient computational approach than previous ones. This paper presents the results of such a study, and includes a thorough discussion of the computational strategy, with particular emphasis on the implementation of an oct-tree data-structure, which is unfamiliar to most physicists. To our knowledge, oct-trees have not yet been applied to this sort of problem, and we hope that our application of them will convince readers of the utility of sparse data-structures in complex problems of computational physics.

The rest of this paper is organized as follows: in the second section we outline our Monte Carlo method and illustrate how the oct-tree data-structure works. When appropirate, we also draw comparison draw comparisons with the methods used in previous work. The third section is devoted to the presentation and analysis of our results. In the last section, we give our conclusions.

2. Monte Carlo algorithm and oct-tree data-structure

Our Monte Carlo procedure generates SARS on a cubic lattice in a grand canonical ensemble at fixed plaquette fugacity β. Thus, the statistics of the generated surfaces can be derived from a partition function of the form

$$Z(\beta) = \sum_S |S|^x \beta^{|S|} = \sum_{n=6}^{\infty} n^x N(n) \beta^n. \tag{3}$$

The inclusion of the integer exponent x in the weighting function amounts to taking the xth derivative of the partition function with $x = 0$. If the value of x is increased,

the percentage of larger surfaces in the distribution is enhanced, but autocorrelation times also increase, as described in section 3.1. As pointed out in [19] and explored in section 3.2, only when x is at least $3/2$ does the distribution of surface areas peak at non-zero $|S|$. More importantly, we show that x must be above $1/2$ in order for the simple analysis procedure of [14] to be viable. Except for one run at $x=2$, we have used $x=3$ in this study. As in [9, 19], our algorithm is a refinement of the Monte Carlo procedure first introduced by Sterling and Greensite [14]. Given a surface S, an attempt to modify it is made by searching for elementary cubes of the lattice having at least one face belonging to S. If such a cube is found, we reverse the status of each of its six faces, regarding whether or not each belongs to the surface S. This process leads to a new surface S', which can be accepted only if it turns out to obey the geometrical and topological constraints imposed on the model. If the constraints are satisfied, then the acceptance of the new surface is subject to satisfaction of the usual Metropolis condition consistent with the grand canonical fugacity β in the partition function.

In [14] the search for cubes was made by sweeping through all those contained in a $10\times10\times10$ box. In subsequent studies [9, 19], the search was restricted to the set of cubes with at least one face belonging to the surface. In this way, surfaces fitting in a $20\times20\times20$ box could be generated. This box still imposes a rather severe finite-size limitation. These approaches are inefficient in that a well defined location in computer memory must be reserved for each cube in the box, whether or not it actually touches the surface. We can, however, store information about the surface configuration using a sparse data-structure, the oct-tree, in which memory is only used for those cubes which actually touch the surface, while all others can be ignored. This procedure allows us to escape the restriction that surfaces fit in a finite box.

Before describing the data-structure explicitly, we comment on the way in which our grand canonical weight in the partition function (3) is actually obtained. In [9, 19], each move of the surface was made by selecting randomly among the cubes having faces in common with it. If we denote by $\|S\|$ the number of such cubes for a surface S, the random choice implies a factor $1/\|S\|$ in the transition rate from S to any configuration S' accessible from S. Detailed balance then clearly implies that the grand canonical weight for a surface S should contain a factor $\|S\|$. Here we prefer to proceed in a way such that $|S|$, rather than $\|S\|$ factors appear in the grand canonical weight, as anticipated in (3). Thus, in our case the first random choice is made within the set of all $|S|$ elementary plaquettes of S. We then choose one of the two cubes sharing this plaquette and perform the usual inversion operation on it. Since this process allows the same cube to be chosen with more than one plaquette choice, we must unbias the procedure so that each distinct possible modification of S has an equal a priori probability. Again, calling S' the surface produced by inversion of the chosen cube, the move $S\Rightarrow S'$ actually has probability $\kappa_{SS'}/|S|$ in the biased procedure, where $\kappa_{SS'}$ is the number of different plaquettes in S the choice of which can lead to the selection of the cube in question.

We can get rid of this bias if we slow down the rate by a factor of $1/\kappa_{SS'}$ by the usual Metropolis procedure of stopping the transition if a random number chosen in $[0, 1]$ is greater than $1/\kappa_{SS'}$. In order finally to obtain the weight in (3), we have to apply at least one further slowing-down process.

In fact, our calculation inserts two filters. The first determined by the ratio

$$\frac{|S|}{|S|+|S'|}$$

in all cases, and the second by

$$\frac{|S'|^x}{|S|^x+|S'|^x}\beta^{|S'|-|S|}$$

in case $|S'|>|S|$, and otherwise

$$\frac{|S'|^x}{|S|^x+|S'|^x}.$$

In this way we get a transition rate for an allowed move $S\to S'$ that is of the form

$$\omega(S\to S')=\begin{cases}A(S,S')|S'|^x\beta^{|S'|-|S|} & \text{if } |S'|>|S| \\ A(S,S')|S'|^x & \text{if } |S'|\leqslant|S|\end{cases} \tag{4}$$

where

$$A(S,S')=A(S',S)=\frac{1}{|S|+|S'|}\,\frac{1}{|S|^x+|S'|^x}.$$

Detailed balance then clearly implies that the equilibrium probability of a surface $|S|$ is proportional to $|S|^x\beta^{|S|}$, consistent with (3).

In our runs, the probability of occurrence of a surface with $|S|=n$ is

$$P(|S|=n)=\frac{N(n)n^x\beta^n}{\sum_{l=6}^{\infty}l^xN(l)\beta^l}. \tag{5}$$

Unlike the simulations reported in [6, 9, 19], we do not keep one plaquette of the surface fixed. In those simulations, the fixed plaquette served to increase x effectively by one. Another increase of one compared to [14] was achieved in [9, 19] by sweeping only over the surface rather than the whole box. (Note, however, that we do not allow the last remaining cube of a surface to vanish, so that we always have $n\geqslant 6$.)

As has been mentioned, we have been able to perform simulations that generate very large configurations, because we use a sparse data-structure, the oct-tree. Oct-trees are a data-structure for storing information about 3D space. Briefly stated, the oct-tree data-structure represents a cube of arbitrary size. The same amount of computer memory can represent a physically small cube as well as a large one. Part of each cube's data-structure denotes whether the cube is empty, full, or partially full. If the cube is empty or full, there is nothing else to describe. If the cube is partially full, it is divided into eight sub-cubes (figure 1), hence the term 'oct'. Each of these may in turn be either empty, full, or partially full. This description is continued recursively until all partially full octs are described in terms of empty or full octs, or until some desired degree of resolution has been reached. This hierarchical representation of a volume is an oct-tree. The first oct in the tree is called the oct-root. For the purposes of our work, the term 'cube' refers to a unit cube of the lattice (i.e. an oct of the finest resolution). To illustrate the labelling of cubes, we present in figure 1 an example of a configuration with a volume of three cubes.

The present use of oct-trees is quite different from the typical one. The ordinary implementation starts with a single oct that represents the total working volume. The oct is divided as objects of importance are discovered in the workspace. This is carried out recursively down to whatever resolution is required. Our representation task is similar, but instead of splitting octs to get more resolution, we double the linear dimension of octs when our volume grows. The finest level of resolution is fixed at

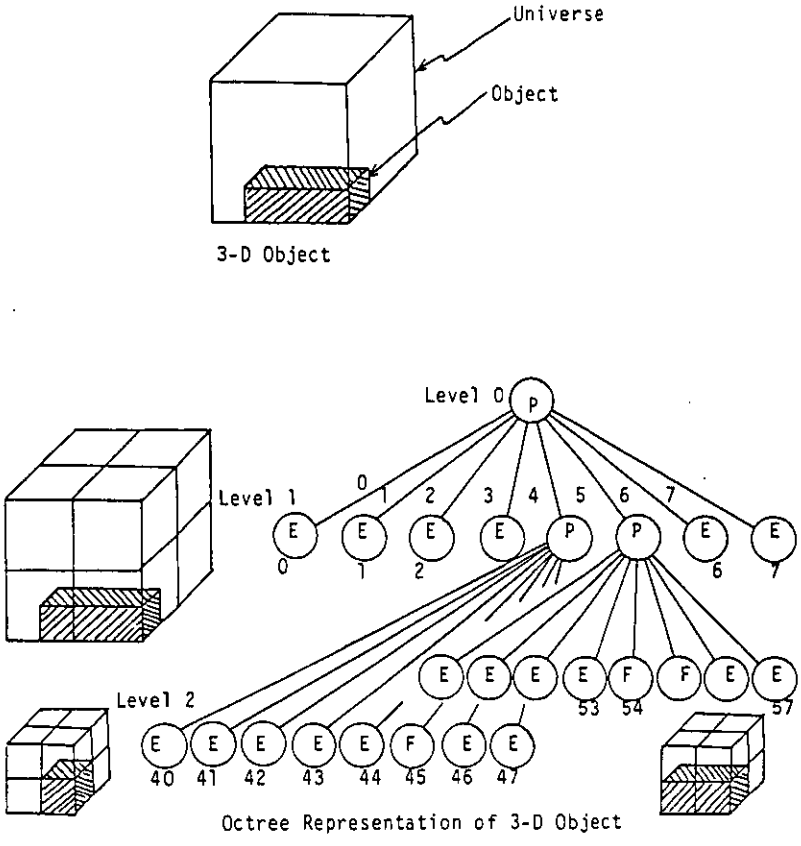

Figure 1. Illustration of the oct data-structure, with successive divisions of cubes into eight sub-cubes. As a specific example, description of a three-cube object is shown to require two levels below the root (i.e. 'grandchilren'). *E*, *P* and *F* denote empty, partially filled and full, respectively.

the unit cube throughout the calculation, but the working volume is not fixed. When a cube appears outside of the oct-tree, we create a new root for the tree that is large enough for the new object. The old root oct becomes one of the children of the new root oct. When an oct's eighth child is filled, the oct is marked as full and all storage previously used to store the children is released. Each parent notices when its last child has become full and executes the same procedure. This recursive process keeps the actual amount of storage in the oct-tree to a minimum. An inverse process occurs when an oct's only child is deleted. The oct is marked empty and space reserved for children is released. This is also executed recursively, as each parent notices when its last child had become empty and releases space no longer used.

Functionally, all an oct consists of is pointers to children. For application to SARS, we have augmented this with a parent pointer, a single coordinate to identify one corner of the oct in space, and a count of the number of children in the current oct. We have also augmented the oct structure so that it stores any faces that lie on the surface. This is easily done with a six-element bit map for the six possible faces on each cube.

One procedure is of special interest because it is the most heavily used and illustrates a particularly nice feature of the oct-tree in physical simulations: **oct-find** is used to

find the oct at a given coordinate. Since the height of the oct-tree is logarithmic with the size of the lattice, searching is very efficient. Starting at the root, the procedure compares the coordinate to the midpoint in each direction. With three comparisons, the appropriate sub-oct is located within which the x, y, z coordinate is guaranteed to lay. This process is recursively repeated until we arrive at the correct cube. As we step down through the oct-tree, the linear dimension of the working volume is halved in each direction. Thus, the search time is

$$O(3\log_8(n)) = O(\log_2(n)) \tag{6}$$

i.e. a binary search. Thus, if it takes k steps to execute **oct-find** in a $2\times2\times2$ lattice, it takes $5k$ steps to do so in a $32\times32\times32$ lattice, and only $20k$ steps in a $1\,048\,576\times 1\,048\,576\times 1\,048\,576$ lattice. An expanded presentation of many aspects of this section is given in [22].

3. Monte Carlo results and their analysis

3.1. Maximum likelihood determination of μ and θ

We performed extensive Monte Carlo runs on Convex C120, IBM RS6000 and SGI computers, generating surfaces consistent with the equilibrium partition function (3) for various values of β below the actual critical value of the model $\beta_c = \mu^{-1}$, which in [19] was 0.577 ± 0.002. It is crucial that we have $\beta < \beta_c$ to prevent the surface from growing without bound. Figure 2 shows three of the distributions we obtained from runs of 10^9 Monte Carlo steps (MCS) for $x = 3$. In earlier work [14], a smaller value of β (0.531) was needed because of the stringent finite-size limitation. Karowski [20] examined many values of β between 0.53 and 0.54.

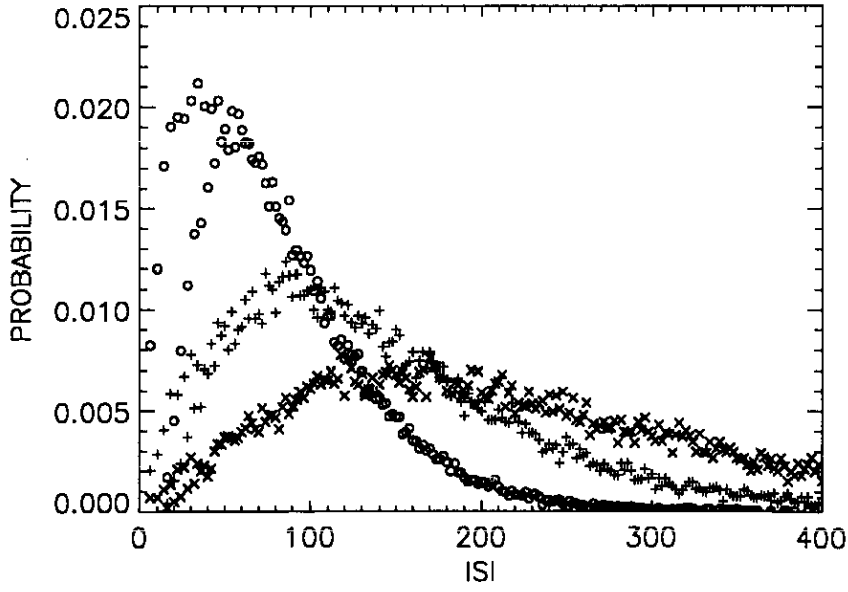

Figure 2. Plots of distributions of occurrences of surfaces as a function of their area, normalized by the total number of occurrences, for $\beta = 0.56$ (○), 0.568 (+), and 0.572 (×). In each case, $x = 3$.

As seen in figure 2 and implicit in (3), the distribution of surface areas should peak at larger values of n as β increases. Likewise, at fixed values of β the distribution of surface areas should peak at larger values of n as x increases. This behaviour was corroborated in a plot similar to figure 2 of distributions from runs at $\beta = 0.56$ with $x = 2$ and 3. Thus, runs with $x = 3$ have the advantage of sampling a relatively higher percentage of surfaces with high $|S|$; for this reason in all other runs with different values of β we chose $x = 3$. Interestingly, this is also the disadvantage of using larger x: since the mean configuration size is larger, autocorrelation is amore serious problem.

To be certian our observed configurations were statistically independent, we used 50 000 MCS between samples for runs with $\beta \geqslant 0.565$. It should be pointed out that the estimate of correlation time reported in [9] and [19] for $\beta = 0.56$ is more optimistic than ours. There, sampling was done every 5000 MCS, an interval about one-fourth the size of our estimated correlation time for this case. We estimated that the correlation time increases with an exponential law as $\beta \to \beta_c = \mu^{-1}$. It is also apparent from figure 2 that for relatively small n (less than about 50), there are actually two distributions: there are far more surfaces with areas n that are odd multiples of 2 than even multiples (and in fact none with $|S| = 8$ or 12). This observation is related to the fact that not every value of $|S|$ is possible (e.g. only 6, 10 and 14 can occur for small configurations). This is reflected in the bimodal values in the plots of effective exponents versus $n_{\min}$ discussed below.

Using the maximum likelihood method, we analysed the distributions like the ones depicted in figure 2 to extract estimates for θ and μ for different values of β. Application of this method to self-avoiding walks is discussed extensively in [23]. It was used by [9, 19] for our SARS problem. In the simplest mode, one assumes the relation (1) is strictly satisfied for $n > n_{\min}$. Pursuant to this assumption, one observes the 'experimental' expectation values of the two quantities

$$O_1(S) = |S|\Theta(|S| - n_{\min}) \tag{7}$$

and

$$O_2(S) = \ln(|S|)\Theta(|S| - n_{\min}) \tag{8}$$

where Θ is the Heaviside unit step function. The maximum likelihood estimates of μ and θ are then obtained as solutions of the pair of equations

$$\langle O_1 \rangle_{\text{obs}} = \langle O_1 \rangle_{\text{th}} \tag{9}$$

$$\langle O_2 \rangle_{\text{obs}} = \langle O_2 \rangle_{\text{th}} \tag{10}$$

where the left-hand sides are the computed Monte Carlo expectation values, while on the right-hand sides we insert the theoretical expectation values based on (1), assumed valid for $n \geqslant n_{\min}$

$$\langle O_1 \rangle_{\text{th}} = \frac{\sum_{n \geqslant n_{\min}}^{\infty} O_1(n) n^{-\theta} \mu^n \beta^n}{\sum_{n \geqslant n_{\min}}^{\infty} n^{-\theta} \mu^n \beta^n}. \tag{11}$$

The numerical solution of this nonlinear system requires great care. For instance, the computed Monte Carlo expectation values require summing over many terms of widely differing magnitudes. To avoid roundoff and truncation difficulties in processing (9) and (10), we needed to use all terms—presorted—on the left-hand sides and 1000 terms on the right-hand sides. Sums were computed in double precision. The nonlinear equations themselves present a more serious difficulty: let $F(\mu, \theta)$ be the (two-component) difference between the right- and left-hand sides of (9) and (10). Figure

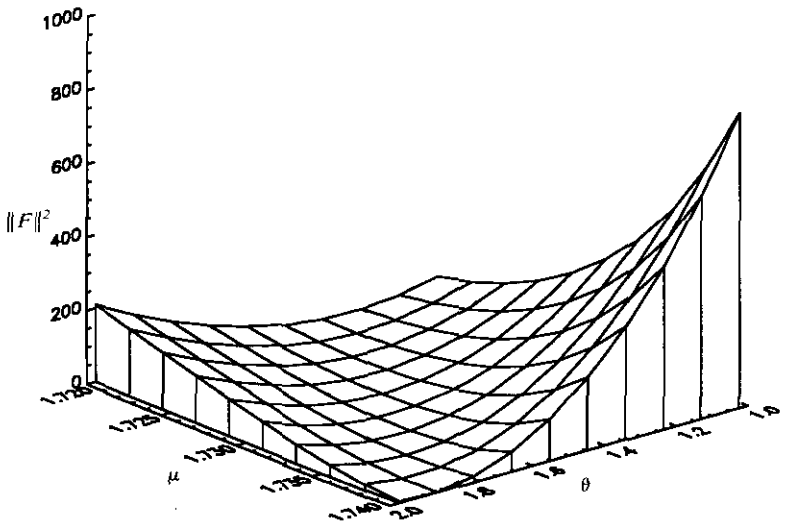

Figure 3. *Illustrative plot of squared difference* $\|F\|^2$ *between observed and predicted distributions of areas, versus* μ *and* θ*, implicitly used in maximum likelihood estimates of these two exponents. Note that the straight, diagonal trough foretells that errors in the two exponents should track each other, but with much greater fluctuations in the former. See text for details. This plot is from an early run with* $x = 2$.

3 is a plot of $\|F\|^2$ as a function of μ and θ for $\beta = 0.56$. The flat 'trough' running roughly north-east to south-west contains the minimum of $\|F\|$. Along this trough, large changes in (μ, θ) cause only small changes in $\|F\|$ so that the minimum is difficult to locate. (This behaviour is typical of the systems of equations arising from the use of maximum likelihood for exponential families [24].) We carried out this calculation in double precision, using the NAG routine SNSQ.

We obtained estimates of θ and μ for different values of β and $x = 3$ for many different values of $n_{\min}$. In principle, the higher $n_{\min}$, the closer the result should be to the correct asymptotic value. Indeed, corrections of the order of $1/n_{\min}$ can be expected, as well as possibly more dominant corrections to scaling arising from deviations from the asymptotic behaviour of relation (1).

In figure 4, we display our determinations of μ and θ for $\beta = 0.56$, $x = 3$ and for $n_{\min} = 0$ and 2, mod 4. Evidently the cases with $n_{\min}$ a multiple of 4 converge to the asymptotic value from below while the others converge from above. Hence, a simple extrapolation would be quite noisy. In the figure we see that the convergence is improved when $n_{\min} > 40$; by extrapolation, we estimate that $\mu = 1.731 \pm 0.002$. Similar sharp estimates, consistent with this value, are obtained from runs at larger β. Figure 4 also shows that the fluctuations in θ follow those in μ, but amplified by two orders of magnitude, as might be expected because of the entropic nature of this exponent, to be discussed below. Thus, it is not feasible to obtain a very precise estimate of θ; but one can see that, roughly, $\theta = 1.5 \pm 0.1$. Extrapolation of the data for θ in figure 4, i.e. with the fitting form $\theta + \text{constant} \times n_{\min}^{-1}$, still does not produce precise results; in contrast, [9] and [19] used only the first four odd-multiple-of-two data points and obtained smoother curves, but none the less quoted comparable error bars. For runs at larger β the estimates of θ are generally within these error bars, but usually well below 1.5. Figures 5 and 6 show similar results for μ and θ, respectively, obtained at

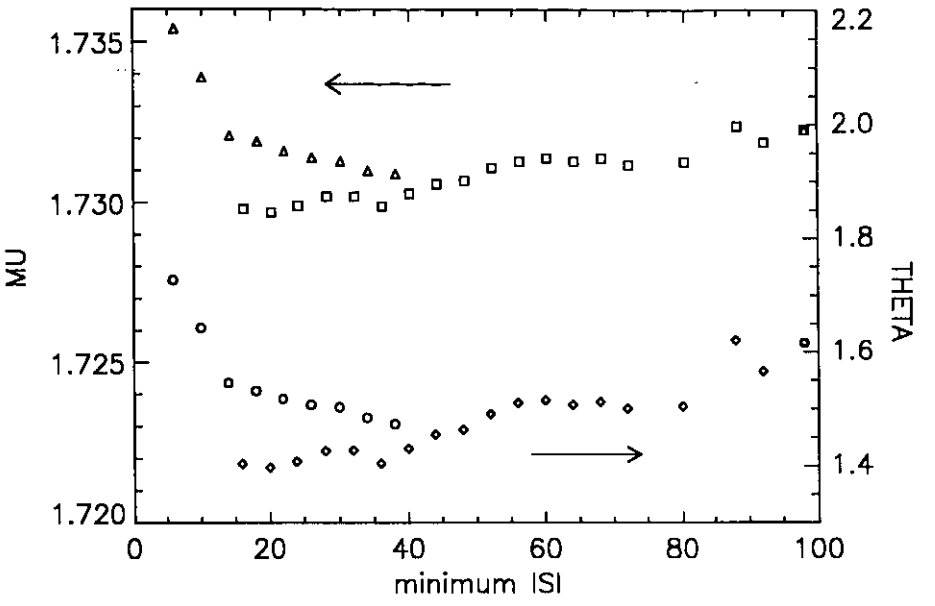

Figure 4. Plots of the exponents μ and θ, determined by maximum likelihood methods at $\beta = 0.56$, versus n_{min}. Referred to the left ordinate, the values of μ for n_{min} an odd or an even multiple of 2 are denoted by △ and □, respectively. Referred to the right ordinate, the values of θ for the lower cut-off an odd or an even multiple of 2 are denoted by ○ and ◇, respectively. While the vertical grids differ by two orders of magnitude, the variations track each other.

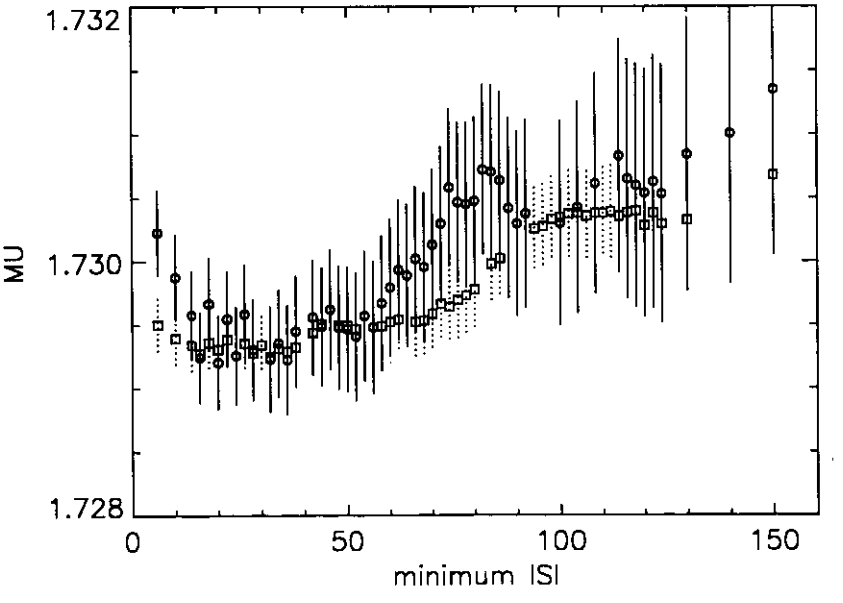

Figure 5. Plot of μ versus n_{min} for $\beta = 0.568$ (○) and $\beta = 0.572$ (□). Error bars are indicated by full and dotted lines, respectively.

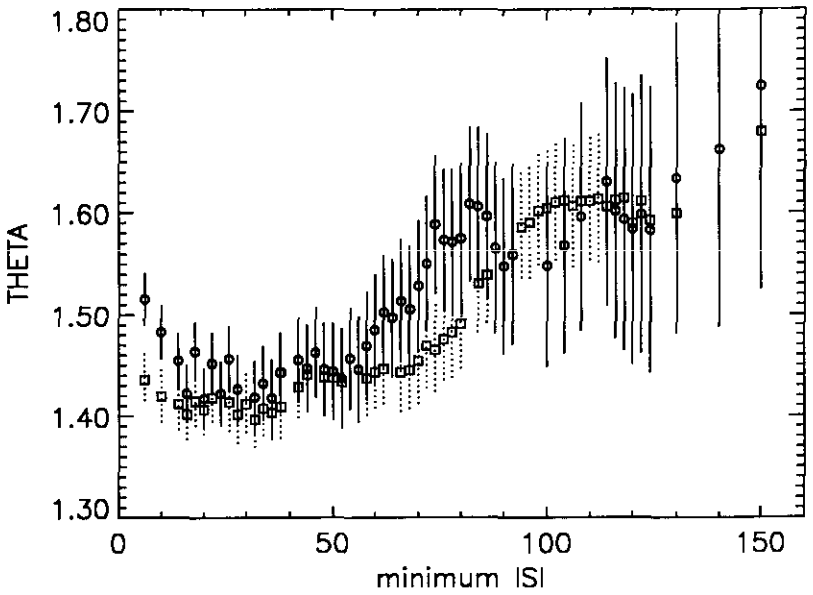

Figure 6. Plot of θ versus n_{min}. The symbols have the same meaning as in figure 5.

$\beta = 0.568$ and 0.572. The situation for θ seems to be due to the extremely flat character of $F(\mu, \theta)$ already mentioned above. Close inspection shows that again the variations in estimates of θ track those of μ, albeit on a much larger scale. The key point is that θ is associated with $\ln n$ while μ is associated with n. This difference is built into the function F and amplifies the variation in the estimates of θ due to noise in the data. Ultimately, this is a consequence of the fact that the derivative of $\ln x$ is $1/x$, which becomes small for large x.

We conclude that the maximum likelihood method is not able to lead to a very precise determination of θ. Taking a naive statistical attitude, we estimated θ as an average of the various extrapolations obtained from all our runs at different β. The crude result is $\theta = 1.39 \pm 0.10$, where the uncertainty reflects the discrepancies among different runs. For μ the final estimate obtained from the same strategy turns out to be $\mu = 1.729 \pm 0.002$.

Given the large statistical errors in θ, we did not even attempt to estimate the possible influence of corrections to scaling.

3.2. Determination of θ and μ via scaling plots

Following the approach of Sterling and Greensite [14]–but mindful that our definition of β is the negative logarithm of theirs—we consider

$$\beta \frac{\partial}{\partial \beta} \ln Z(\beta) = \langle |S| \rangle \tag{12}$$

with Z given in (3). In the limit $\beta \to \beta_c^-$, we can make a continuum approximation for the summation in Z. Using the asymptotic form of $N(n)$ in (1), we find

$$Z(\beta) \sim \frac{\Gamma(1+x-\theta)}{[\ln(\beta_c/\beta)]^{1+x-\theta}}. \tag{13}$$

So from (12) we can conclude that

$$\langle |S| \rangle \underset{\beta \to \beta_c^-}{\sim} (1+x-\theta)\frac{\beta_c}{\beta_c-\beta}. \tag{14}$$

Notice that this continuum-based result makes sense only if the prefactor of the divergence, $1+x-\theta$, is positive. With a $\theta \simeq 1.5$, as found below, (14) would not be correct for $0 \leqslant x < 0.5$. In that case, the leading singular term in (13) would not be divergent, and (14) should be replaced by a singularity $\propto [\beta_c/(\beta_c-\beta)]^{2+x-\theta}$, with $2+x-\theta < 1$. In [14] the analysis of θ was based on (14), but with $x=0$. This inconsistency, in our opinion, explains the serious discrepancies between our determinations θ and β_c and those reported by Sterling and Greensite [14]. Figure 7 shows our plot of $\langle |S| \rangle^{-1}$ as a function of β, based on the distributions from the runs at different β mentioned in section 3.1. The reciprocal of the intercept on the x-axis gives μ, while the value of θ can be easily extracted from the slope of a straight line superimposed on the data. It is remarkable how linear the data become in this plot. An estimate of the slope gives $\theta = 1.500 \pm 0.026$, while $\mu = 1.729 \pm 0.036$, reasonably consistent, although somewhat higher than the maximum likelihood estimate. The error bars for θ and μ are obtained by propagating the standard deviations of the individual data points, as estimated from the fluctuations between independent runs. Due to the high degree of consistency of the results, this method appears to be more reliable—certainly more stable—for θ than that in section 3.1. Accordingly, we based our final estimates of θ and μ on this method.

An alternative approach makes use of the scaling properties of the entire distribution of surface areas rather than just average value. To the extent that the asymptotic expressions are valid, it should be possible to rescale these distributions for the various

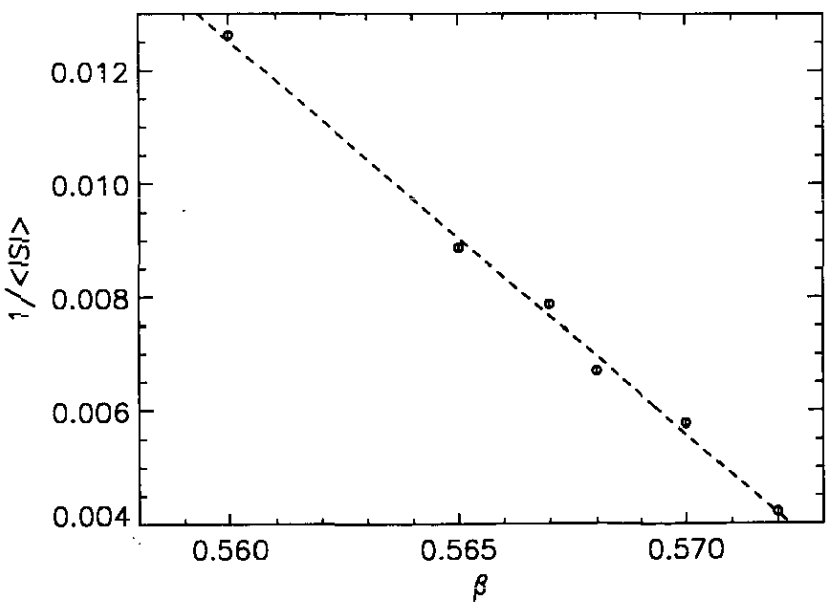

Figure 7. Plot of $\langle |S| \rangle^{-1}$ versus β. The best fit, determined by linear regression, is shown by the broken line. The error bar for each point is about the size of the small circle. In this analysis [14], the intercept with the x-axis gives $1/\mu$, while the value of θ can be easily extracted from the slope of fitted straight line. See text.

values of β and x, as displayed individually in figure 2, so that the data collapse to a single universal curve. Specifically, simple differentiation with respect to n shows that the mode of the distribution occurs at [9, 19]

$$n_{\max} = \frac{x-\theta}{\ln(1/\beta\mu)}. \tag{15}$$

For $x < \theta$, the maximum would be at the smallest allowed $|S|$, viz 6.

We have already noted the failure of the continuum approximation when $x < \theta - 1$. The frequency of occurrence of the mode, $N_{\max} \equiv N(n_{\max})$, for the *normalized* distribution can then be readily evaluted using (1) and (13), and simplified to

$$N_{\max} = \frac{-\ln(\beta\mu)[(x-\theta)e^{-1}]^{x-\theta}}{\Gamma(1+x-\theta)}. \tag{16}$$

By then plotting $N(n)/N_{\max}$ versus $n/n_{\max}$, the data collapse neatly to a single curve, especially away from the extremities. To further bring out the dependence on θ, we next removed by hand the well characterized term $(\beta\mu)^n$, leaving $n^{(x-\theta)}$ and inviting a log-log plot. Accordingly, we plot in figure 8 $[\ln(N(n)/N_{\max}) - n\ln(\beta\mu)]$ versus $\ln(n/n_{\max})$. The data overall collapse impressively. The slope of the linear part, predicted to be $x-\theta$, is consistent with the values of θ discussed earlier, but there is sufficient spread that the method does not easily distinguish between 1.4 and 1.5, for example. For small surfaces we see clearly a bifurcation into separate curves for those surfaces which have area a multiple of 4 and those which do not. For large surfaces we observe greater noise in the data and have truncated the high end to omit spurious scatter.

3.3. Exponent ν and asymptotic ratio $n/V(n)$

The exponent ν could be estimated more straightforwardly using linear regression.

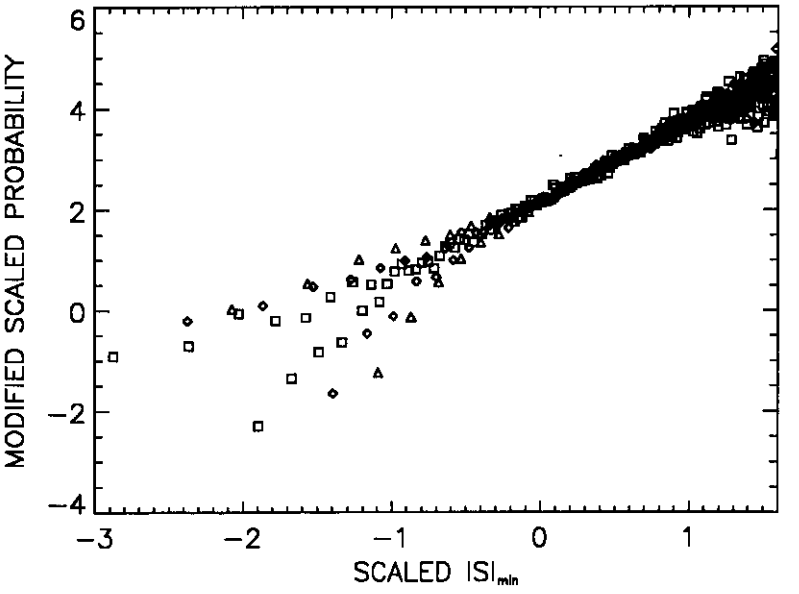

Figure 8. Log-log plot of scaled probability, modified to remove the well characterized dependence on $\beta\mu$, versus surface area normalized by its mode, for $\beta = 0.56$ (△), 0.565 (◇) and 0.57 (□).

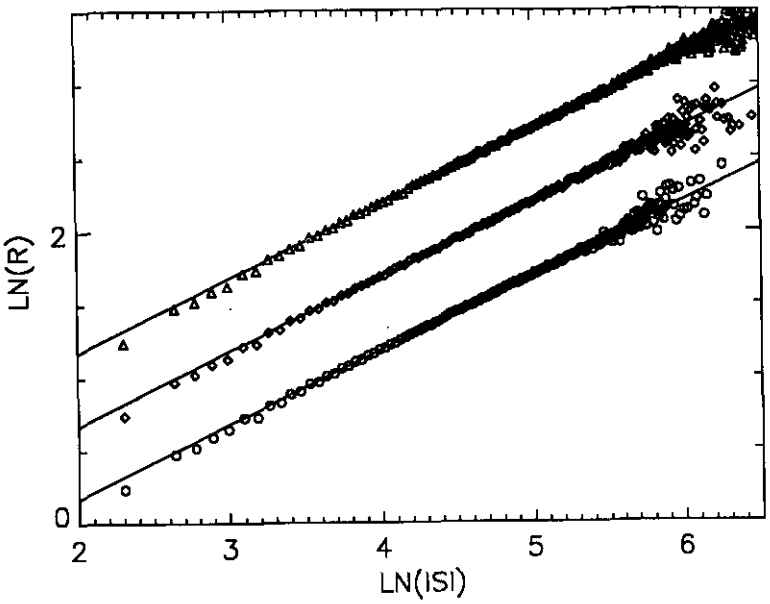

Figure 9. Log-log plots of radius of gyration versus surface area for $\beta = 0.56$ (○), 0.565 (◇) and 0.57 (□). The ordinate scale refers to the results for $\beta = 0.56$; the other two were displaced upward by 0.5 and 1.0 respectively. The straight lines were determined by linear regression over the range of minimal scatter; all have slope within 0.001 of 0.510.

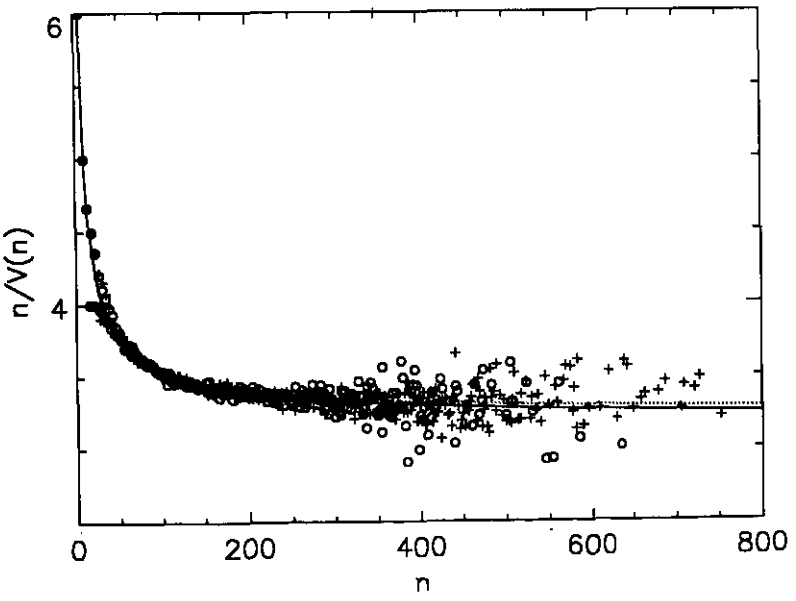

Figure 10. Plots of $n/V(n)$ versus n for runs with $\beta = 0.565$ (○) and $\beta = 0.568$ (+). Three-parameter fits to the form $a + bn^{-c}$, with values of a being 3.16 and 3.22, are shown as full and dotted curves, respectively.

Figure 9 shows, for several β, our Monte Carlo results for the root mean square radius of gyration, $R(n)$, of surfaces with $|S| = n$. In each case, the log–log plot becomes linear rapidly, suggesting that the asymptotic regime has been reached. Again, we had to discard data for small n as non-asymptotic and for large n because of poor statistics. Using only the 'best' data, usually for $\ln(n)$ between 3.4 and about 5.5, the slope for a half-dozen different β or x was invariably with 0.001 of 0.510. On the other hand, this range is rather limited. For a broader range, there is much greater variation, from around 0.515 down to somewhat below 0.500. Averaging over the values obtained in all the runs and discarding just the first 15 points led to an estimate for ν of 0.506 ± 0.007, while by dropping the runs for the largest two β lowers the average to 0.503 without changing the error bars. Taken together, an estimate for ν of 0.509 ± 0.004 seems reasonable. This value is slightly above the estimate in [9, 19], which was consistent with $\frac{1}{2}$. Our data range did not allow a meaningful search for systematic errors, particularly for correction-to-scaling exponents.

As already mentioned in the introduction, the surface-to-volume ratio is an important quantity to characterize the SARS. To obtain this ratio, we found it most convenient to evaluate, as a function of n, the average volume $V(n)$ enclosed in sampled surfaces with $|S| = n$. From the these data for $n/V(n)$, we can then estimate the asymptotic value in the limit $n \to \infty$. Figure 10 show plots of $n/V(n)$ versus n for runs at different β. There is very strong evidence that the ratio asymptotically approaches a non-zero value which we estimate to be 3.18 ± 0.03. This number was obtained by averaging, for several different β, the results of least-squares fits using the functional form $a + bx^{-c}$; c was between 0.68 and 0.78.

4. Concluding remarks and perspectives

The results discussed in section 3 are obtained from statistics involving surfaces with areas nearly an order of magnitude larger than those considered in [9, 19]. We could achieve this closer approach to the asymptotic limit by removing the box constraint and by considering distributions with relatively high x and with β very close to β_c. Higher values of x, or β even closer to the estimated β_c than those considered here, would have enriched the sampling of high n, but at the price of inconveniences, such as longer correlation times. Our choice of β and of x seemed a reasonable compromise in view of our computational capabilities. Only one set of calculations has been reported that seems to involve surfaces larger than ours [20], and we seriously question the statistical significance of those results (cf [9]). In [20] determination of ν was accomplished by using very large surfaces generated with β close to the β_c of 0.531 previously determined by [14], which is considerably lower than our estimate of 0.578 for β_c. Especially with such a small β, the sampling of very large surfaces (n near 5000) appears to us to be quite problematical.

Our estimates of ν are basically consistent with—albeit slightly larger than—the value of Glaus and Einstein [9, 19] and strongly corroborate the conjecture that our self-avoiding surfaces have the same exponent, $\nu = \frac{1}{2}$, as that expected for branched polymers in 3D. The determination of θ by maximum likelihood involved greater uncertainty; the value is less decisively in the universality class of branched polymers, and we feel that within this method a definitive conclusion about this exponent, unfortunately, cannot be reached, even after our extensive analysis. This tentative outlook contrasts with the more optimistic conclusions drawn in [9, 19]. We have

shown here that the maximum likelihood approach, on which they relied exclusively to determine θ, gives results which are not only rather erratic but also do not become significantly sharper for samplings closer to the asymptotic limit. For a more reliable estimate of θ the simpler kind of analysis described in section 3.2 appears more appropriate, and gives θ reasonably close to $\frac{3}{2}$, as expected for branched polymers [15]. As explained above, the reason why the similar analysis of [14] did not give the results we found is primarily the inconsistency between (14) and the choice $x=0$.

Another advance in our results is the relatively high degree of confidence about the extrapolation of $n/V(n)$. A ratio of this $(\langle |S|/V \rangle)$ form, averaged over all but the bottom of the distribution at $\beta = 0.56$, was tabulated in [19]. The entries were for distributions truncated at several different small values of $n_{\min}$. A subsequent extrapolation [9] produced the estimate 3.5, suggesting that the tabulated data were not close enough to the asymptotic limit to warrant such extrapolation, but none the less indicative of a non-vanishing limit. As anticipated in the introduction, this more important idea that the ratio remains above zero indicates that our surfaces enclose a region with fractal dimension not higher than $1/\nu$ and is an indication that ramified tubular configurations with tubes of minimal size presumably dominate in the RS statistics. This picture is consistent with the evidence from ν and θ that the problem belongs to the branched polymers unviersality class. It is more difficult to interpret the value ~ 3.2 of the asymptotic ratio. If this number were 4, topological considerations would indicate that asymptotically the surfaces do not include internal points, i.e. lattice points enclosed by the surface but not on the surface.

It is interesting to note that bond lattice trees without loops in $d=3$ have a critical bond fugacity of about 0.10 [26]. Our β_c, raised to the power 3.2, gives 0.17, i.e. a number of the same order as the above critical fugacity. Thus, it probably makes sense to view the elementary cubes within the surface as playing a role similar to that of effective bonds in a branched polymer problem.

Recent theoretical arguments [21], however, suggest that a very important role could be played by topology in determining critical behaviour, as long as one restricts the consideration to closed surfaces (empty boundary). Analytical results indicate that, as soon as one considers surfaces which are closed, but have an unrestricted number of handles (i.e. an arbitrary genus), the enclosed volume should grow asymptotically as R^3, rather than as $R^{1/\nu}$, as we found here for restricted topology (in our case $1/\nu \simeq 2$). Thus, changing the topological constraints apparently can alter the universality class of a closed surface. No numerical verification of the above conjecture has appeared to date; in particular, a determination of ν and θ for closed SARS with unrestricted topology is needed. Suitable modifications of our algorithms can be efficiently used to investigate such an issue, and work is already in progress on this line.

The results of this paper, particularly the strong indication that SARS realize the critical behaviour of branched polymers in the scaling limit, leads to an obvious question: what are the requirements of a SARS model in order that it represents a genuine fractal surface in the scaling limit rather than a linear, even if highly ramified, object? We think that one way to achieve different critical behaviour without relaxing topological constraints is to enrich the model by allowing a local interaction with an effect analogous to an extrinsic curvature dependence in the continuum. For example, an appropriate fugacity could be introduced to control the number of links joining plaquettes not lying in the same plane. If coplanar adjoining plaquettes are sufficiently favoured over plaquettes joining at right angles, it seems likely that a more compact structure than branched polymers should appear in the simulations. Thus, one could

possibly observe interesting multicritical phenomena in this generalized model as the fugacity is varied. The study of such multicritical phenomena might well reveal new universality classes for the generalized model. In [25] a model has recently been discussed in which effects similar to those postulated for the above local interaction are provided by the inclusion of annealed Ising vacancies in the problem.

Acknowledgments

TLE and ALS received funding for international collaboration from NATO Grant No 86/0782. TLE is also partially funded by NSF Grant DMR 88-02986. We thank Isabel Beichl for numerous helpful interactions. ALS and TLE also benefitted from discussions with N C Bartelt.

References

[1] Balian R, Drouffe J M and Itzykson C 1975 *Phys. Rev.* D **11** 2104
[2] Drouffe J M and Itzykson C 1979 *Phys. Report* **38C** 133
[3] Wilson K 1974 *Phys. Rev.* D **10** 2445
[4] Maritan A and Stella A 1984 *Phys. Rev. Lett.* **53** 123
[5] Durhuus B, Fröhlich J and Jonsson T 1983 *Nucl. Phys.* B **225 [FS9]** 185
[6] Durhuus B, Fröhlich J and Jonsson T 1984 *Nucl. Phys.* **240 [FS12]** 453
[7] Kantor Y, Kardar M and Nelson D R 1986 *Phys. Rev. Lett.* **57** 791
[8] Sokal A 1989 private communication
[9] Glaus U 1988 *J. Stat. Phys.* **50** 1141
[10] Hammersley J M 1961 *Proc. Camb. Phil. Soc.* **57** 516
[11] Fröhlich J 1985 *Applications of Field Theory of Statistical Mechanics* (*Lecture Notes in Physics 216*) ed L Garrido (Berlin: Springer)
[12] Maritan A and Stella A 1987 *Nucl. Phys.* B **280 [FS18]** 561
[13] Drouffe J M, Parisi G and Sourlas N 1979 *Nucl. Phys.* B **161** 397
[14] Sterling T and Greensite J 1983 *Phys. Lett.* **121B** 345
[15] Parisi G and Sourlas N 1981 *Phys. Rev. Lett.* **46** 871
[16] Redner S 1985 *J. Phys. A: Math. Gen.* **18** L723; 1986 **19** 3199
[17] Glaus U 1986 *Phys. Rev. Lett.* **56** 1996
[18] See also, eg, Cates M E 1985 *Phys. Lett.* **161B** 363
[19] Glaus U and Einstein T L 1987 *J. Phys. A: Math. Gen.* **20** L105
[20] Karowski M 1986 *J. Phys. A: Math. Gen.* **19** 3375
[21] Banavar J R, Maritan A and Stella A L 1991 *Science* **252** 825
[22] Libes D 1989 NIST Internal Report 89-4055 submitted for publication
[23] Berretti A and Sokal A 1985 *J. Stat. Phys.* **40** 483
[24] Rosenblatt J 1989 private communication
[25] Maritan A, Seno F and Stella A L 1991 *Phys. Rev.* B **44** 2834
[26] de Gennes P G 1985 *Rev. Mod. Phys.* **57** 827